Ultracompact polarization converter with a dual subwavelength trench built in a silicon-on-insulator waveguide

Aitor V. Velasco[2,4], María L. Calvo[2], Pavel Cheben[1,5], Alejandro Ortega-Moñux[3], Jens H. Schmid[1], Carlos Alonso Ramos[3], Íñigo Molina Fernandez[3], Jean Lapointe[1], Martin Vachon[1], Siegfried Janz[1], and Dan-Xia Xu[1]

[1]*Institute for Microstructural Sciences, National Research Council Canada, Ottawa, Ontario K1A 0R6, Canada*

[2]*Departamento de Optica, Facultad de Ciencias Fisicas, Universidad Complutense de Madrid, 28040 Madrid, Spain*

[3]*ETSI Telecomunicación, Universidad de Málaga, 29071 Málaga, Spain*

[4]*e-mail: avillafr@pdi.ucm.es*

[5]*e-mail: pavel.cheben@nrc.ca*

Received October 24, 2011; revised December 1, 2011; accepted December 5, 2011; posted December 7, 2011 (Doc. ID 156835); published January 20, 2012

The design and fabrication of an ultracompact silicon-on-insulator polarization converter is reported. The polarization conversion with an extinction ratio of 16 dB is achieved for a conversion length of only 10 μm. Polarization rotation is achieved by inducing a vertical asymmetry by forming in the waveguide core two subwavelength trenches of different depths. By taking advantage of the calibrated reactive ion etch lag, the two depths are implemented using a single mask and etching process. The measured converter loss is −0.7 dB and the 3 dB bandwidth is 26 nm.

OCIS codes: 130.3120, 130.5440, 230.7380.

Recent developments in integrated silicon photonic devices have demonstrated the remarkable capabilities of the silicon-on-insulator (SOI) platform to implement a wide range of applications, such as optical interconnects [1], nonlinear photonics [2], biological sensors [3], and microspectrometers [4]. However, while the high refractive index contrast of the SOI platform is advantageous for high-density photonics integration, it comes with a drawback of largely disparate propagation characteristics for the TE- and TM-like modes. As a result, most of the photonic devices in SOI have been designed for a single mode and a single polarization, typically TE. To mimic polarization independent operation, polarization diversity schemes are typically used with the polarization splitters and rotators as the key components.

Recently, several SOI polarization rotators (also known as mode converters) have been proposed, including designs based on triangular waveguides [5], asymmetric waveguides with two etch depths [6], coupling via an intermediate multimode waveguide [7], waveguides with vertical and sloped sidewalls [8], and a combination of horizontal and vertical waveguides [9]. However, fabrication of these devices is often complex, with multiple patterning and etching steps involved. Some single-etch devices have also been reported, such as a polarization rotator based on an adiabatic taper and an asymmetrical directional coupler [10] (conversion length 100 μm), and a mode converter based on the cross-polarization coupling effect [11] (conversion length 44 μm). Additionally, mode converters with single [12] or multiple [13] trenches etched to create an asymmetric waveguide have been implemented in gallium arsenide (GaAs) waveguides, reaching a 96% mode conversion within a device of 150 μm. Some numerical simulations have also been performed in an attempt to extend the single-trench design to silicon waveguides [14].

In this Letter, we report the design and fabrication of an ultracompact dual-trench polarization rotator in SOI, with a conversion length as short as 10 μm, for a wavelength of 1.5 μm. The converter schematic is shown in Fig. 1. The converter exploits the asymmetry induced by two adjacent subwavelength trenches, resulting in two orthogonal hybrid modes (Fig. 1, inset) with optical axes rotated 45° with respect to the x and y axes, that is, hybrid modes consisting of 50% TE and 50% TM polarization. This geometry allows both hybrid modes to be excited with equal efficiency by a TE (or TM) polarized input. The two hybrid modes propagate with different propagation constants along the device, resulting in a 90° polarization rotation at each half-beat length $L_{1/2}$:

$$L_{1/2} = \frac{\pi}{\Delta\beta}, \tag{1}$$

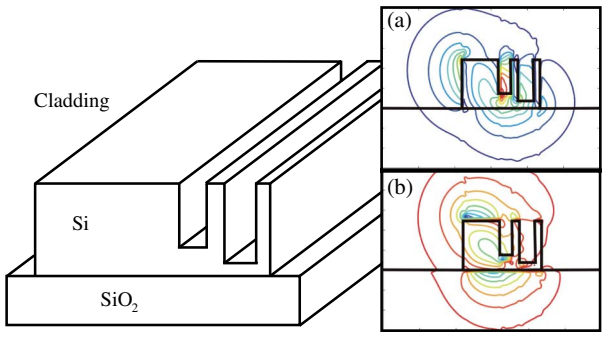

Fig. 1. (Color online) Schematic structure of the proposed polarization converter. (Inset, color online) Simulated contour plot of the (a) X and (b) Y components of the field of the first hybrid mode for a dual-trench structure with trench widths 60 nm and 85 nm and trench depths 210 nm and 235 nm, respectively.

where $\Delta\beta = \beta_1 - \beta_2$ is the difference between the propagation constants of the two hybrid modes, β_1 and β_2, respectively. Additionally, in order to reach conversion efficiency values close to 100%, the power distributions of the two hybrid modes should efficiently overlap, and the higher order mode conversion needs to be minimized. Indeed, the operation mechanism of the converter ensures reciprocity between TE-TM and TM-TE mode conversion. The dual-trench structure is chosen, as opposed to a single-trench design, in order to optimize mode conversion and dramatically reduce device length.

To design the polarization rotator, we define a dual-trench subwavelength structure in the waveguide with variable depths and widths, and we perform two-dimensional (2D) mode computation with a commercial software (FIMMWAVE, Photon Design, UK). The full width of the Si-wire waveguide was chosen as 450 nm, for single mode operation near 1.5 μm wavelength. The Figure 1 inset shows the calculated hybrid mode profiles for this geometry. 2 μm-long linear inverse taper mode adaptation sections were included at both ends of the polarization rotator to ensure a smooth transition between the wire waveguide and the dual-trench waveguide, and to generate equal excitation of the two hybrid modes.

Insofar as the width and depth of the two trenches are considered independent design parameters, modes with a 45° offset can be obtained for many combinations of these parameters (Fig. 2(a)). For a given wavelength, greater trench widths require shallower trench depths and result in shorter conversion lengths (Fig. 2(b)). Also, a greater disparity in the depths of the two trenches results in greater conversion lengths (Fig. 2(c)). Simulations predict that if the width and depth of one of the trenches are increased, the size of the other trench has to be reduced to achieve maximum conversion efficiency, and conversion length is altered. The problem to minimize the device size and/or to maximize the conversion efficiency can be solved numerically. However, only a restricted set of solutions is suitable for device fabrication. In order to fabricate two narrow trenches of different depths using a single-etch step, we take advantage of the reactive ion etch (RIE) lag effect, i.e., the etch depth dependence on the trench width for small feature sizes.

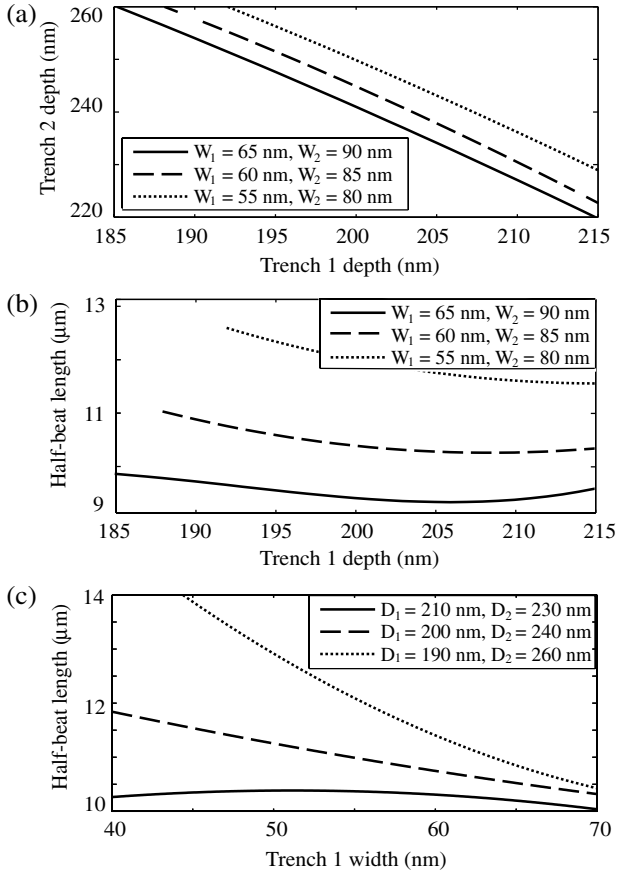

Fig. 2. (a) Combinations of trench depths (D_1, D_2) that yield hybrid modes with 45° offset, for different combinations of trench widths (W_1, W_2). (b) $L_{1/2}$ versus depth of the first trench and (c) $L_{1/2}$ versus width of the first trench, for parameter combinations yielding hybrid modes with 45° offset.

For our fabrication process, a reduced etched depth is observed for a feature size smaller than ~140 nm. We calibrated the RIE lag effect using scanning electron microscopy (SEM) measurements on a set of reference trenches of varying width, obtaining the calibration curves shown in inset of Fig. 3. By applying the calibration curve to the set of theoretical solutions for trench widths and depths yielding hybrid modes with 45° offset, we found the optimized values for the two trench widths of 60 nm and 85 nm and trench depths of 210 nm and 230 nm, respectively. This structure yields a final device length of 10.3 μm. Parameter combinations that result in shorter conversion lengths cannot be fabricated, as they do not match the RIE lag calibration curve, and resulting trench depths would be too shallow.

The operation wavelength can be increased by increasing the trench width and depth and/or the overall device length. According to our dimension tolerance study, a 13 nm shift of the design central wavelength is predicted for fabrication errors of 9 nm in the depths of the trenches or 5 nm in the widths of the trenches. Our calculations show that the design can be optimized for 1550 nm wavelength by enlarging the outer trench to a width of 90 nm and a depth of 240 nm. For that wavelength and topology, conversion length is increased to 12.74 μm.

Samples were fabricated using SOI substrates with a 0.26 μm thick silicon and a 2 μm thick buried oxide layer. Waveguides with the polarization rotator structure were defined in a single patterning step by electron beam lithography with high contrast hydrogen silsesquioxane (HSQ) resist. Inductively coupled plasma reactive ion

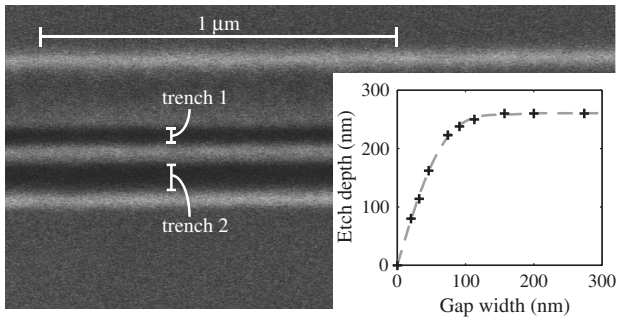

Fig. 3. SEM of the fabricated dual-trench polarization converter. (Inset) Etch depth versus gap width due to RIE lag effect.

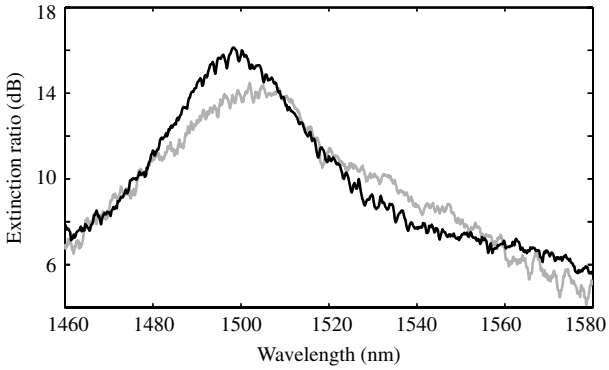

Fig. 4. Measured ER versus wavelength of the fabricated device for TE to TM (black) and TM to TE (gray) mode conversion.

etching (ICP-RIE) was used to transfer the resist pattern into the silicon layer. Figure 3 shows a SEM image of the fabricated device.

The polarization rotator was characterized using a tunable laser over a wavelength range of 1460–1580 nm, with polarization control optics. The light was coupled both at the input and the output of the chip using lens fibers facing the chip facets terminated at both sides with subwavelength grating mode converters [15]. The output signal was separated into the TE and TM components with a polarizing beam splitter, and both polarization components were measured independently.

The measured extinction ratio (Eq. (2)) is shown in Fig. 4.

$$\mathrm{ER}_{\mathrm{TE\text{-}TM}} = 10 \cdot \log \frac{P_{\mathrm{TM}}}{P_{\mathrm{TE}}}, \tag{2}$$

where P_{TM} and P_{TE} are the output powers of the TM and TE polarized fundamental modes. Measured extinction ratio was corrected by calibrating polarization dependent loss in the 60 μm-long strip waveguide between the device and the chip facet (0.4 dB/cm excess loss for TE polarization). Furthermore, the polarization dependence of the output coupling efficiency between the subwavelength grating mode converter and the lensed fiber of the light collecting system was compensated (0.3 dB excess loss for TM polarization). Polarization conversion effects in the subwavelength grating mode converter were calibrated by performing polarization-resolved measurements of a bare waveguide with the mode transformers, showing that polarization was maintained with an extinction ratio exceeding 35 dB. Polarization conversion effects in the adaptation stages were characterized by measuring the polarization rotation angle for a set of test devices with different lengths, showing a rotation in the adaptation stage of 2°, which was corrected by a 0.22 μm reduction in the length of the rotator. Trench depths measurements of the adaptation section, determined by RIE lag effect, confirmed shallow trenches during most of the adaptation stage.

The peak extinction ratio for TE-TM conversion is 16 dB (97.5% conversion efficiency, defined as $\eta_{\mathrm{TE\text{-}TM}} = P_{\mathrm{TM}}/[P_{\mathrm{TM}} + P_{\mathrm{TE}}] \times 100\%$) at the nominal wavelength of 1500 nm. A peak extinction ratio of 14 dB is observed for TM-TE conversion, showing a slight drop due to polarization dependent losses in the device and to fabrication imperfections. The measured extinction ratio 3 dB bandwidth is 26 nm, while a conversion efficiency over 90% is reached within a bandwidth of 47 nm. Polarization converter loss was estimated by subtracting the insertion loss of a reference waveguide without a polarization converter, to compensate for the fiber-chip coupling losses and the loss of the Si-wire interconnecting waveguide. The measured polarization converter excess loss is –0.7 dB, with an adaptation stage excess loss of –0.4 dB.

In conclusion, we have demonstrated the design and fabrication of an ultracompact and efficient polarization rotator using a dual subwavelength trench in an Si-wire waveguide. The device is implemented in a single-etch step standard fabrication process. Extinction ratios up to 16 dB were reached for an ultrashort conversion length of 10 μm, opening promising prospects for device applications for efficient polarization management in integrated optoelectronic circuits.

Financial support from the Spanish Ministry of Science and Innovation (MICINN) is acknowledged under grants TEC2008-04105 and TEC2009-10152.

References

1. A. Liu, L. Liao, Y. Chetrit, J. Basak, H. Nguyen, D. Rubin, and M. Paniccia, in *Proceedings of the Fifth International Conference on Group IV Photonics* (2008), pp. 368–370.
2. M. A. Foster, A. C. Turner, J. E. Sharping, B. S. Schmidt, M. Lipson, and A. L. Gaeta, Nature **441**, 960 (2006).
3. A. Densmore, D.-X. Xu, P. Waldron, S. Janz, P. Cheben, J. Lapointe, A. Delâge, B. Lamontagne, J. H. Schmid, and E. Post, IEEE Photon. Technol. Lett. **18**, 2520 (2006).
4. P. Cheben, J. H. Schmid, A. Delâge, A. Densmore, S. Janz, B. Lamontagne, J. Lapointe, E. Post, P. Waldron, and D.-X. Xu, Opt. Express **15**, 2299 (2007).
5. J. Yamauchi, M. Yamanoue, and H. Nakano, J. Lightwave Technol. **26**, 1708 (2008).
6. D. Vermeulen, S. Selvaraja, W. Bogaerts, and G. Roelkens, presented at the Seventh International Conference on Group IV Photonics, Beijing, China, 2010, paper WC6
7. Y. Yue, L. Zhang, M. Song, R. G. Beausoleil, and A. E. Willner, Opt. Express **17**, 20694 (2009).
8. C. Brooks, P. E. Jessop, H. Deng, D. O. Yevick, and G. Tarr, Opt. Eng. **45**, 044603 (2006).
9. J. Zhang, T. Y. Liow, M. Yu, G. Q. Lo, and D. L. Kwong, Opt. Express **18**, 25264 (2010).
10. D. Dai and J. E. Bowers, Opt. Express **19**, 10940 (2011).
11. L. Liu, Y. Ding, K. Yvind, and J. M. Hvam, Opt. Lett. **36**, 1059 (2011).
12. S. H. Kim, R. Takei, Y. Shoji, and T. Mizumoto, Opt. Express **17**, 11267 (2009).
13. B. M. Holmes and D. C. Hutchings, IEEE Photon. Technol. Lett. **18**, 43 (2006).
14. D. M. H. Leung, B. M. A. Rahman, and K. T. V. Grattan, IEEE Photon. J. **3**, 381 (2011).
15. P. Cheben, P. J. Bock, J. H. Schmid, J. Lapointe, S. Janz, D.-X. Xu, A. Densmore, A. Delâge, B. Lamontagne, and T. J. Hall, Opt. Lett. **35**, 2526 (2010).